Dalton Transactions

An international journal of inorganic chemistry

Accepted Manuscript

This article can be cited before page numbers have been issued, to do this please use: G. E. Gomez, C. A. López, R. L. Ayscue, K. Knope, M. D. R. Torres Deluigi and G. Narda, *Dalton Trans.*, 2019, DOI: 10.1039/C9DT02109D.

ROYAL SOCIETY OF CHEMISTRY

rsc.li/dalton

View Article Online
DOI: 10.1039/C9DT02109D

ARTICLE

Strong photoluminescence and sensing performance of nanosized $Ca_{0.8}Ln_{0.1}Na_{0.1}WO_4$ (Ln=Sm, Eu) compounds obtained by dry "top-down" grinding method

Received 00th January 20xx,
Accepted 00th January 20xx

DOI: 10.1039/x0xx00000x

Germán E. Gomez,*[a] Carlos A. López,*[a] R. Lee Ayscue III [b], Karah E. Knope [b], María del R. Torres Deluigi [c] and Griselda E. Narda [a]

Two lanthanide doped nanosystems $Ca_{0.8}Ln_{0.1}Na_{0.1}WO_4$ (Ln=Eu, Sm), denoted as **Eu@CWO** and **Sm@CWO**, were prepared by a "top-down" approach in three simple steps which included activation, miniaturization by high-energy milling, and further calcination. The solids were thoroughly characterized by X-ray powder diffraction (XRPD), Raman spectroscopy and scanning-electron microscopy (SEM). Also, analyses of the compounds' structure and the impact of the milling on crystallite shape and size were carried out through Rietveld refinements. The solid-state photoluminescence was studied in terms of excitation, emission, lifetimes (τ_{obs}) and europium-quantum yields. Finally, the **Eu@CWO** sample was employed as potential water-stable chemical sensor towards toxic cations, finding a quenching effect in the presence of iron ions.

Introduction

Studies focused on the optical properties of the lanthanide ions in diverse host materials provide fundamental data that includes energetic transitions, radiative and non-radiative decay processes, intrinsic and overall quantum yields, and lifetimes. Such information is critical for assessing and/or designing optical devices such as lasers, upconverters, color displays, and amplifiers. Towards this end, many recent efforts have aimed to develop new or improved optical devices via the appropriate pairing of host materials (chemical compositions) with doped lanthanide ions.[1–4] Trivalent lanthanide ions are characterized by a gradual filling of the 4*f* orbitals, from $4f^0$ (La^{3+}) to $4f^{14}$ (Lu^{3+}). These electronic $[Xe]f^N$ configurations (N = 0-14) generate a variety of electronic energy levels,[5] resulting in intricate optical properties.[6] Consequently, each lanthanide ion exhibits narrow and characteristic 4*f*-4*f* transitions. All Ln^{3+} ions (except La^{3+} and Lu^{3+}) exhibit *f-f* emissions that range in wavelength from ultraviolet (UV) to visible and near-infrared (NIR) spectral regions. For example, Sm^{3+}, Eu^{3+}, Tb^{3+}, and Tm^{3+} ions can emit orange, red, green, and blue light, respectively, while Nd^{3+}, Yb^{3+} and Er^{3+} ions display the well-known near-infrared luminescence.

The ABO_4 structure (A=Ca, Sr, Ba; B=W, Mo) has been used as traditional host platforms for lanthanide ions. Using this material Gd^{3+}, Er^{3+}, Yb^{3+}@$CaWO_4$[7] or carbon-dots@$CaWO_4$ (or $BaWO_4$) doped with Er^{3+},Yb^{3+} as upconverting (UC) micro/nano materials have been reported.[8] Additionally, $CaWO_4$ has been employed as a matrix for Eu^{3+} and a variety of hierarchical architectures that show red emission under UV excitation were obtained by controlling doping through different synthetic routes.[9–15] Zhou et al. studied and compared the luminescence properties of $CaMoO_4$:Eu^{3+} and $CaMoO_4$:Eu^{3+}-A^+, where A = Li, Na, K, and deduced that Li^+-doped $CaMoO_4$:Eu^{3+} produced the optimal red emission upon excitation at 464 nm.[16] Despite many investigations on $CaBO_4$:Eu^{3+} (B= Mo, W) to the best of our knowledge, extensive research regarding important photophysical parameters such as luminescence lifetime (τ_{obs}) or even quantum yield parameters (QY_{tot} or QY_{Eu}) has not been reported. Yet the τ_{obs} value is an important property to be evaluated for designing new luminescent materials. Furthermore, the potential sensing applications of $CaBO_4$:Ln^{3+} phases are scarcely investigated.[17] Table 1 displays a set of selected lanthanide-doped ABO_4 luminescent phases.

Commonly, ABO_4 phases are synthesized through conventional methods at high temperatures for long periods of times. Additionally, hydrothermal or microwave assisted syntheses have served as an activation process for further calcinations at high temperatures.[18,19] By comparison, the use of high-energy milling for these types of inorganic compounds is scarcely reported.[20] Additionally, sonochemical methods have been employed to obtain luminescent ABO_4 phases as a fast and solvent-free route of synthesis.[21] In this work, we report a novel three-step "top-down" synthesis that follows a "green" methodology through a solvent-free approach with a

[a] *Instituto de Investigaciones en Tecnología Química (INTEQUI). Universidad Nacional de San Luis, CONICET, Almirante Brown 1455, 5700 San Luis, Argentina. E-mails: gegomez@unsl.edu.ar, calopez@unsl.edu.ar*
[b] *Georgetown University, Washington, D.C., USA.*
[c] *Laboratorio de Microscopia Electrónica y Microanálisis (LABMEB), Facultad de Química, Bioquímica y Farmacia, Universidad Nacional de San Luis, Ejército de los Andes 950, 5700 San Luis.*

† Footnotes relating to the title and/or authors should appear here.
Electronic Supplementary Information (ESI) available: tables of Rietveld analysis, f-f transitions assignments, decay profiles, emission spectra and extra micrographies. See DOI: 10.1039/x0xx00000x

final calcination at lower temperatures than those previously reported in the literature.

Table 1: Select ABO_4 lanthanide-doped phases (A=Ca, Sr, Ba; B=W, Mo).

Compound	Synthesis method	Size-particles	Property	Reference
carbon-dots @$CaWO_4$:Yb^{3+}, Er^{3+}	hydrothermal	4 μm	UC	8
Gd^{3+}, Er^{3+}, Yb^{3+}@$CaWO_4$	hydrothermal and further calcination	3-4 μm and 100 nm	UC	7
$CaMoO_4$:Eu^{3+}	co-deposition in the water/oil phase and further calcination	0.12μm-1.79μm	red-emitter	9
$Ca_{0.8}Ln_{0.1}Na_{0.1}WO_4$ (Ln=Sm, Eu)	High energy milling and further calcination	50-150 nm	red and orange emitters/chemical sensing	this work
$CaMoO_4$: Eu^{3+}	nitrate–citrate gel combustion	500 nm-1μm	red-emitter	10
$CaMoO_4$: Bi^{3+}, Eu^{3+}	solid-state reaction and calcination	not reported	red-emitter	22
$CaMoO_4$: Eu^{3+}, Dy^{3+}, Tb^{3+}	flux crystal growth	1-5 mm	red and green emitter	12
$CaMoO_4$: Na^+, Eu^{3+}	solid-state reaction and calcination	not reported	red emitter	13
$CaMoO_4$: Eu^{3+}	sonochemical	6 μm	red emitter	14
$CaWO_4$: Eu^{3+}, Dy^{3+}, Tb^{3+}	sol-gel methodology and nanocasting	not reported	red, green and blue emitters	15
$CaMoO_4$: A^+, Eu^{3+}(A=Li, K, Na)	microwave sintering	3,82 μm	red emitter	16
$CaWO_4$:Eu^{3+}, Tb^{3+}	sonochemical	120-160 nm	cathodo- and photo-luminescence	21
$CaWO_4$:Er^{3+},Yb^{3+}	solid-state reaction and calcination	~1-4 μm	thermal sensing	17
$CaWO_4$: Eu^{3+}	hydrothermal	4 μm	red-emitter	18
$CaWO_4$: Eu^{3+}	high energy milling and further calcination	not reported	red-emitter	20
$CaWO_4$: Eu^{3+}	microwave	not reported	red-emitter	16

In this work, we synthesized $Ca_{0.8}Ln_{0.1}Na_{0.1}WO_4$ (Ln=Eu, Sm) (namely as **Eu@CWO** and **Sm@CWO**) samples via a simple three step method that included two mechanochemical treatments followed by a soft calcination process. Double doping (e.g. $0.5Ln^{3+}0.5Na^+$ for Ca^{2+}) was required to maintain electroneutrality in the scheelite structure and to obtain a defect-free compound. The nanosized solids were characterized by X-ray powder diffraction and scanning-electron microscopy. Structural analysis was carried out by Rietveld refinements which provided information about crystallite size. The solid-state photoluminescence (SSPL) was analysed by recording the excitation and emission spectra and calculating the τ_{obs} from the decay profiles. Also, the europium-quantum yields were measured. Finally, the **Eu@CWO** sample was evaluated as potential sensor towards toxic cations.

Experimental

Synthesis

The title materials were obtained through a novel three step-synthesis. Unlike traditional synthetic routes, this methodology does not use solvent and has a relatively low calcination temperature; thus, achieving a "green" method to obtain optical materials. $Ca_{1-2x}Ln_xNa_xWO_4$ samples, with x = 0 and 0.1 and Ln = Eu and Sm, were obtained as white powders by employing a mechanothermal method, where the solid-state reaction was mechanically activated by high-energy milling in a planetary ball mill. The starting reagents were $CaCO_3$, Eu_2O_3 (or Sm_2O_3) Na_2CO_3 and WO_3. The ball milling processes were carried out using a Fritsch Pulverissette 6 planetary ball mill equipped with a cylindrical tungsten carbide vial (80 cm^3) together with 15 mm diameter WC balls. The ball mass–powder mass ratio was 29:1, the rotation speed was 500 rpm, and the milling time was 1 h in intervals of 15 minutes. From these conditions, the weight-normalized cumulative kinetic energy (E_{cum}) was calculated to be 0.2 $kJ{\cdot}g^{-1}$ according to Rojac *et al.*[23] After this mechanical activation, the samples were calcined for 1 h at 700 °C which produced pure and well-crystallized phases with the scheelite structure type. To obtain miniaturized powders, an aliquot of both samples was re-milled under the same conditions described previously, but with a ball mass–powder mass ratio of 40:1 over 8 h, yielding an E_{cum} of 2.2 $kJ{\cdot}g^{-1}$. These reduced size samples were used for luminescent characterizations. A schematic view of the synthesis procedure is illustrated in scheme 1.

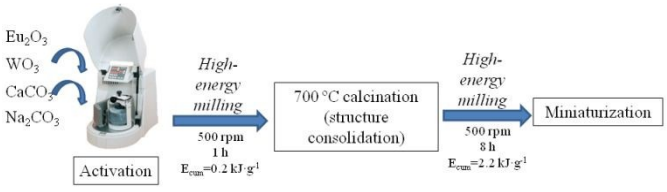

Scheme 1: Synthesis of **Ln@CWO** compounds.

X-ray powder diffraction (XRPD)

The identification and characterization of the solid phases were carried out by laboratory XRPD using a Rigaku Ultima IV diffractometer with CuKα (λ = 1.5418 Å) radiation. The patterns were refined by the Rietveld method using the FullProf program.[24,25] The profile shape was modelled using the Thompson-Cox-Hastings pseudo-Voigt function[26], and the instrumental resolution parameters were considered in the refinements in order to obtain the microstructural parameters.

Scanning Electron Microscopy (SEM)

Images were obtained on a Zeiss LEO1450VP instrument; samples were placed on adhesive carbon tape coated with gold. SEM images were also collected with a Zeiss SUPRA 55-VP scanning electron microscope at an acceleration voltage of

30 kV with an in-lens detector. The samples were mounted directly onto conductive carbon "Lift-N-Press" adhesive tabs. Dispersion was completed by introducing 2 mg of sample into 2 mL of n-hexanes and then sonicated for 45 minutes.

Photoluminescence spectra and lifetime measurements

Photoluminescence measurements were obtained on solid samples at room temperature using a Horiba PTI QM-400 system. Excitation and emission spectra as well as lifetimes were collected on ground solid powders crushed between two glass slides. Time-resolved lifetime measurements were acquired using a Xenon flash lamp as the average of 10,000 shots. Reported lifetimes and standard deviation are the average of three collections.

Quantum yields determinations

Quantum yields were collected for **Eu@CWO** using an 8.9 cm integrating sphere coated in Spectralon fluoropolymer. Samples were ground to homogenous powders and loaded into a Teflon sample holder placed within the sphere. Slit widths were maintained at 1 nm, and the spectra recorded were background-corrected using a blank sample holder and corrected for the wavelength dependence of the spectrofluorometer, sampling optics, and integrating sphere. Reported quantum yields are averages of three independent determinations.

Chemical sensor studies

The sensing activity of the Eu-based compound was investigated by monitoring the emission at 616 nm, when exciting the samples at 393 nm. A quartz cuvette with an optical path of 1 cm was employed. Stock aqueous solutions of 200 ppm of each metal (Cu^{2+}, Fe^{2+}, Zn^{2+}, Co^{2+}, Mn^{2+}, UO_2^{2+}, Th^{4+}, Pb^{2+} and Hg^{2+}) were prepared. Suspensions were prepared by introducing 1.5 mg of powdered sample into 4 mL (0.37 mg·mL^{-1}) of each metal stock solution. The samples were previously ultrasonicated for 15 minutes. The excitation and emission slits were set at 1.5 nm.

Results and discussion

Crystal structure

The structural identification and characterization of all samples were performed from XRPD data for well-crystallized, milled samples. All samples were indexed to the scheelite structure ($CaWO_4$), and no impurities were observed. Moreover, as illustrated in Figure 1, milling resulted in a strong line broadening associated with microstructural effects for the Eu-doped sample.

All XRPD patterns were refined in the tetragonal space group $I4_1/a$(88).[27] In the scheelite structure the W metal center is located in a tetrahedral site; Ca is coordinated by eight oxygen atoms. Each CaO_8 polyhedron edge-shares with four other polyhedra; WO_4 tetrahedra are distributed between these sites. The results of the Rietveld refinement of well crystallized samples is summarized in Table S1. For doped phases, the Ca/($Ln_{0.5}Na_{0.5}$) ratio was refined, and the site occupancies are in accordance with the expected stoichiometry: $Ca_{0.8}Ln_{0.1}Na_{0.1}WO_4$. The microstructural analysis of these samples does not suggest a peak broadening being indicative of a large size of crystallite.

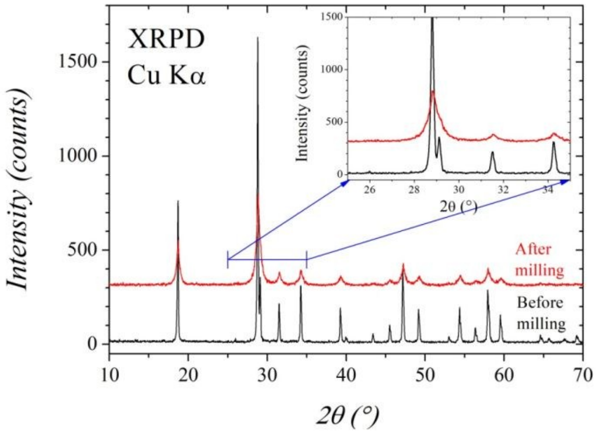

Figure 1: Effect on the XRPD pattern of grinding method of **Eu@CWO** nanoparticles.

The milled samples were further refined with special attention given to line broadening. As mentioned previously, the line shape was modelled using the Thompson-Cox-Hastings pseudo-Voigt function. The U, V, and W parameters are fixed and correspond to the instrumental broadening; hence, only the Lorentzian isotropic strain (X) and size (Y) were refined. From these parameters, the apparent size and strain were calculated from the Scherrer and Stokes-Wilson formula, respectively. Figure 2 shows the best fits for the Ln doped phases after milling treatments. Table S2 summarizes the cell and microstructural parameters of these samples. No appreciable change in the observed cell parameters after milling suggests that the size reduction process did not modify the crystallographic features of lanthanide-doped scheelite structure type. Furthermore, the apparent size and strain of crystallite is similar in both samples. Obtained strain parameters are high and in accordance with a milling process that generates grains with a distorted surface. The crystallite size of ~18 nm is greatly reduced with respect to well crystallized samples.

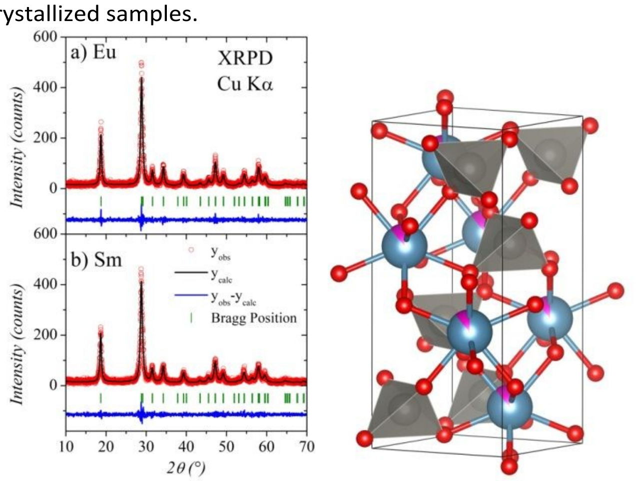

Figure 2: Refinement for **Eu@CWO** and **Sm@CWO** (left). Observed (red points), calculated (black full line) and difference (bottom) Rietveld profiles for both compounds at 298 K. **Eu@CWO** refined structure (right), with Ca (blue), Eu/Na (pink), W(grey), and O (red)

Morphology analysis

The morphology characterization was carried out by SEM and Rietveld analysis in order to study the impact of the synthesis approach on the obtained particle sizes. From SEM analysis, the averaged particle sizes were found into the 300-400 nm and 50-150 nm ranges for the samples before and after miniaturization "top-down" treatment (Figures 3 and S1-3). However, according to Figure 3, a high grade of crystalline aggregation was achieved. . Basing on the Rietveld refinement analysis of **Ln@CWO** nanosystems (Table S2), it was possible to state that each particle is composed by crystallites of ~18 nm.

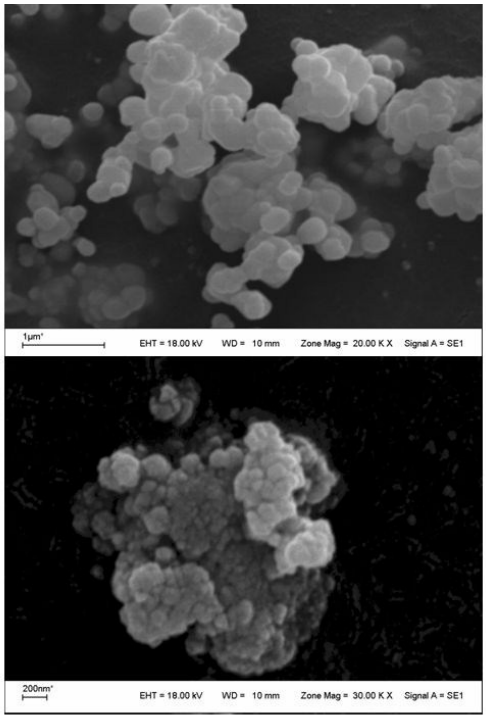

Figure 3: SEM micrographies of **Eu@CWO** before (top) and after (bottom) milling miniaturization.

Solid state photoluminescence (SSPL)

Illustrated in Figure 4, the excitation and emission spectra of host matrix $CaWO_4$ (**CWO**) were studied. The excitation band located at 330 nm is ascribed to a charge transfer band (CTB) associated with an electron transfer from O^{2-} ligand to W^{6+}. The corresponding blue emission is observed as a broad band with a maximum located at 400 nm (see Figure S4).

The excitation spectra of **Sm@CWO** and **Eu@CWO** exhibit broad bands in the 260-350 nm region which are attributed to a CTB (Figures 4 and 5, top). In general, CTBs can arise through three different mechanisms: (i) host absorption which involves electron transfer from O^{2-} ligand to W^{6+} (ii) inter-valence charge transfer due to electronic transition from 4f state of Eu^{3+} (or Sm^{3+}) to W^{6+} and (iii) electron transfer from the filled 2*p* orbitals of O^{2-} anions to the vacant 4*f* orbitals of Ln^{3+}.[28] Such broadness in CTB can potentially be arised by the contribution from all the three types of electronic transition.

Sm@CWO sample shows the $^4G_{5/2} \rightarrow {}^6H_J$ transitions (J=5/2, 7/2, 9/2, 11/2) with a max emission at 646 nm ($^4G_{5/2} \rightarrow {}^6H_{9/2}$) (Figure 4, bottom). The remaining peaks are observed at 564, 608, 706 nm for J=5/2, 7/2, 11/2 respectively. The excitation spectrum shows a complex combination of transitions with maxima at 405 and 482 nm. 1931 Comission Internationale de l'Éclairage (CIE) coordinates of **Sm@CWO** emission are 0.62, 0.37 (x,y) (see Figure 6).

Sample **Eu@CWO** exhibits an emission spectrum with peaks corresponding to the transitions within the Eu^{3+} ion's 4*f* shell, $^5D_0 \rightarrow {}^7F_J$ (J=0-4), with a maximum emission at 616 nm ($^7F_2$). The remaining peaks are positioned at 580, 592, 655 and 702 nm for J=0, 1, 3, and 4 transitions, respectively (Figure 5 bottom). The excitation spectrum shows a complex combination of transitions with maxima at 395, 465 and 535 nm. Notably, the two lower energy transitions are exceptionally deep into the visible region (Figure S5 and S6). 1931 CIE Coordinates of **Eu@CWO** are 0.66, 0.33 (x,y) (Figure 6). The corresponding assignment of the 4*f*–4*f* excitation transitions for **Eu@CWO** and **Sm@CWO** are presented in Table S3.

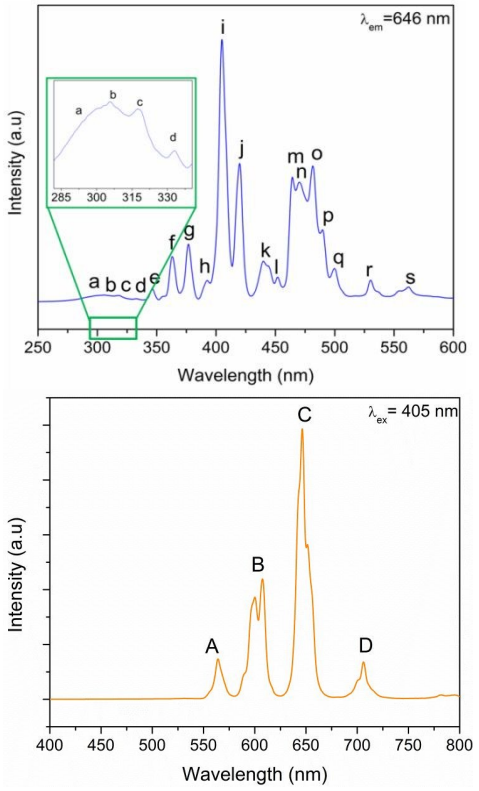

Figure 4: Excitation (top) and emission (bottom) spectra of **Sm@CWO**.

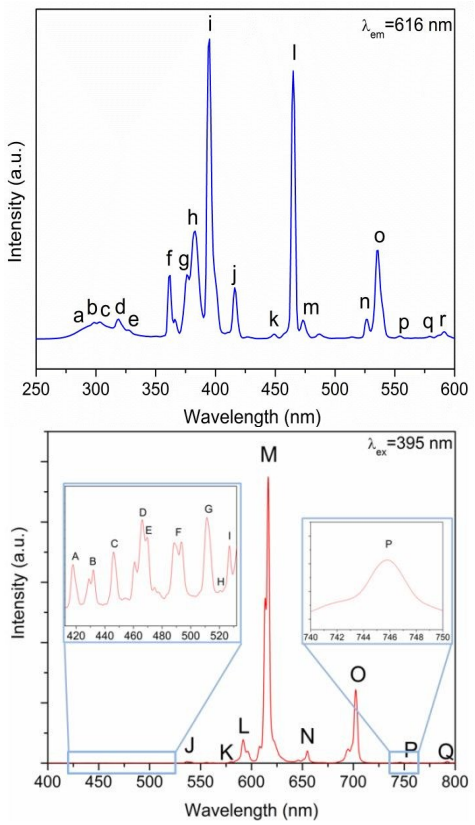

Figure 5: Excitation (top) and emission (bottom) spectra of **Eu@CWO**.

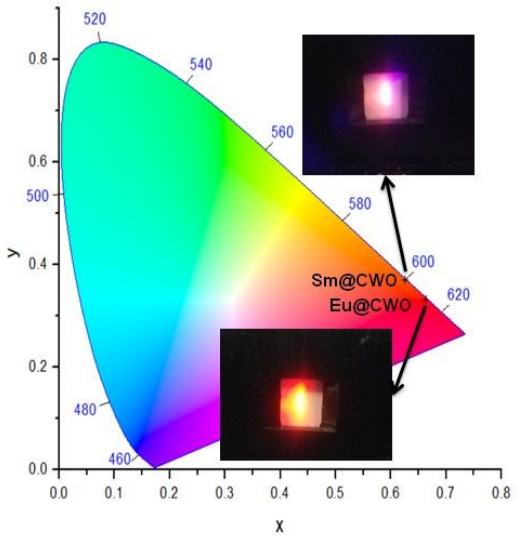

Figure 6: CIE 1931 chromaticity diagram showing the (x,y) color coordinates for **Eu@CWO** and **Sm@CWO** nanoparticles after being excited with the corresponding wavelengths. Pictures show the samples under direct excitation in the fluorometer.

For lifetime measurements, time based decay spectra were collected in triplicate (Figure S7). For **Eu@CWO**, lifetimes were collected at excitation wavelengths of 395, 465, and 535 nm monitoring the emission at 616 nm ($^5D_0 \rightarrow {}^7F_2$) in which all values were consistent. Exponential fitting was modelled between 160-4000 µs to avoid influence of initial excitation and account for estimated zero intensity luminescence. The biexponential fitting (R^2 = 0.9999) (equation 1) revealed average lifetimes (τ_{obs}) of 126 µs and 445 µs.

$$I = A + I_1.e^{-t/\tau_1} + I_2.e^{-t/\tau_2} \quad (1)$$

For the case of **Sm@CWO**, lifetimes were collected at an excitation wavelength of 405 nm monitoring the emission at 646 nm ($^4G_{5/2} \rightarrow {}^6H_{9/2}$). Exponential fitting was modelled between 112-1200 µs to avoid the influence of initial excitation and account for estimated zero intensity luminescence. The biexponential fitting (R^2=0.9984) resulted in average lifetimes of 12 µs and 106 µs.

In both cases, the single exponential fitting showed disagreement with the decay profiles, demonstrated by higher R^2 values than those employing the bifunctional model. This model would suggest the presence of two emitting centres in the structure. This behaviour can be related with the crystallographic features. As it was discussed previously, each Ln^{3+} (in the centre of polyhedron LnO_8) is edge-connected to four AO_8 polyhedra. Considering these features, a statistical analysis revealed that 66% of the lanthanides are isolated, while the other 34% are connected to another emitting centre. Assuming that the lifetime of each Ln^{3+} is affected by the vicinity of another one, the presence of two emitting centres can be assigned to differences in the lanthanide environments.[29]

To qualify the ability of the matrix to sensitize the emission of Eu(III) centres, and to get information of the relationship between the structure and photoluminescence properties, the photophysical parameters of **Eu@CWO** were analysed. These parameters included: the overall quantum yield (QY_{tot}), intrinsic quantum yield (QY_{Ln}), and the efficiency of the matrix-to-metal energy transfer (η_{sens}). The relationship between these terms is given in equation 2.

$$QY_{tot} = QY_{Ln} \bullet \eta_{sens} \quad (2)$$

The total quantum yields (QY_{tot}) were experimentally collected using an integrating sphere and calculated according to equation 3:

$$QY_{tot} = \frac{E_s - E_b}{L_b - L_s} \quad (3)$$

where E_s is the integrated emission spectrum of the sample, E_b is the integrated emission spectrum of the blank (integrating sphere and empty sample holder), L_b the blank absorption, and L_s the sample absorption at the excitation wavelength.

For a correct evaluation of the SSPL efficiency of the Eu-doped sample, the QY_{Ln} was calculated. This parameter expresses how well the radiative processes compete with the non-radiative pathways and provides optimized quantum efficiencies for these materials. Assuming that non radiative (k_{nr}) and radiative (k_r) processes are essentially involved in the depopulation of $^5D_0$ state, the QY_{Ln} can be expressed as:

$$QY_{Ln} = k_r/(k_r+k_{nr}) \quad (4)$$

In general, contributions of the k_{nr} include back-energy transfer to the sensitizer, electron transfer quenching, and quenching by matrix vibrations. Moreover, C-H, O-H, and N-H

View Article Online
DOI: 10.1039/C9DT02109D

vibrations which are commonly found in organic moieties have an important contribution to k_{nr}.[30] The radiative contribution k_r can be calculated from the equation:

$$k_r = 1/\tau_r \quad (5)$$

The so-called radiative lifetime τ_r can be approximated for Eu(III) by the equation[31]:

$$k_r = (1/\tau_r) = A_{MD,0} \bullet n^3 \bullet (I_{tot}/I_{MD}) \quad (6)$$

In equation 6, $A_{MD,0}$ is the spontaneous emission probability of the $^5D_0 \rightarrow {}^7F_1$ magnetic dipole transition equal to 14.65 s^{-1}, n is the refractive index, I_{tot} is the total integrated emission of the $^5D_0 \rightarrow {}^7F_J$ (J= 0-6) transitions and I_{MD} is the integrated emission of the $^5D_0 \rightarrow {}^7F_1$ transition.

If the radiative lifetime, τ_r, is known, QY_{Ln} can be calculated using the observed luminescence lifetime. Based on eqn. (1) and (4), the QY_{Ln} can be calculated as:

$$QY_{Ln} = \tau_{obs}/\tau_r \quad (7)$$

At the same time, knowledge of both τ_{obs} and τ_r enables determination of the overall rate of non-radiative deactivation. Hence, the radiative lifetime is an important parameter in the photophysical description of lanthanide luminescence. The SSPL parameters of **Eu@CWO** are summarized in Table 2.

Sensing studies

In the context of chemical sensor design, Tb^{3+} and Eu^{3+} inorganic compounds have received significant interest due to their *hypersensitive transitions* ($^5D_4 \rightarrow {}^7F_5$ and $^5D_0 \rightarrow {}^7F_2$, respectively). These materials possess optical properties which are readily affected by their chemical and physical environment.[32] During the last fifteen years, Eu and Tb hybrid materials have been extensively used as efficient platforms for sensing ions,[33] water,[34] VOCs (volatile organic compounds),[35] explosives[36] and agrotoxics.[36]

Regarding its water stability and robust emission signal, the chemosensing performance of **Eu@CWO** was investigated by measuring the redPL in presence of cationic species (see Figure 7).

In this study the emission intensities were used as an optical handle for sensing. The emission band centered at 616 nm decreases when **Eu@CWO** is suspended in 200 ppm of metallic solutions (see Figure 7). The quenching efficiency (QE) of the *hypersensitive* transition in the presence of the metals could be calculated as:

$$QE\% = (I_0 - I)/I_0 \bullet 100 \quad (9)$$

where I_0 and I represent the emission intensity values in the absence and presence of the quencher, respectively. Based on these results, Fe^{2+} represents an efficient quencher for the luminescence of **Eu@CWO**, exhibiting a QE of 65%, being the highest value for the set of metal solutions.

The plausible mechanism for luminescence quenching by iron ions has been further investigated. In this context, many reasons for such a quenching effect have been explored: (1) the collapse of the framework, (2) ion exchange between the targeted ions and central metal ions of the sensors or (3) the resonance energy transfer, among the most relevant.[37] According to absorption spectrum of Fe^{2+} solution,[38] it has a large overlap with the excitation spectrum of **Eu@CWO**. Therefore, this overlap of the Fe^{2+} absorption band and the excitation of **Eu@CWO** (395 nm) may be responsible for the quenching effect through the electron-transfer mechanism.

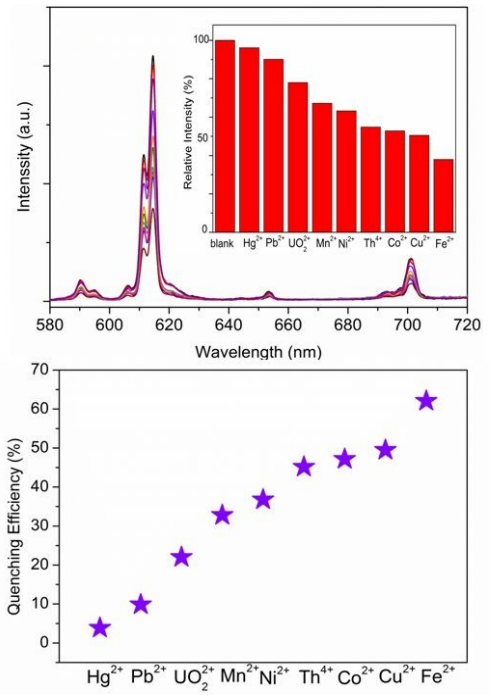

Table 2: Photophysical parameters, measured in triplicated, of the Eu@CWO.

Sample	I_{tot}	I_{MD} ($^7F_1$)	QY_{tot} (%)	QY_{Eu} (%)	η_{sens} (%)	k_{obs} (s^{-1})	k_r (s^{-1})	k_{nr} (s^{-1})	τ_r (µs)	τ_{nr} (µs)
1	78338	6162	2.30	27.97	8.22	2247	629	1619	1591	618
2	75862	6247	1.91	26.72	7.13	2247	600	1647	1666	607
3	75774	6232	2.03	26.75	7.59	2247	601	1646	1664	608
Average ± σ**	76658 ± (1456)	6214± (46)	2.08± (20)	27.15± (72)	7.65± (55)	2247	610± (16)	1637± (16)	1640± (43)	611± (6)

* Assuming average $(\tau_{obs})_{av}$ of 445 µs the following data table is calculated. ** Standard deviation.

Figure 7: Emission of **Eu@CWO** (top) under different metallic suspensions of 200 ppm. Quenching Efficiency of each cation species to the europium hypersensitive transition (bottom).

Conclusions

Two lanthanide nano-systems based on $Ca_{0.8}Ln_{0.1}Na_{0.1}WO_4$ (Ln=Eu, Sm) were successfully prepared by a novel and simple three step methodology including: activation, calcinations, and a "top-down" miniaturization by high-energy milling. The novelty of the synthesis lies in the fact that it is solvent free, implying shorter calcinations times than previously reported methods to obtain analogous phases of nanoparticles with sizes around 50-150 nm. All the compounds were fully characterized by X-ray powder diffraction () and Scanning-electron microscopy (SEM). Moreover, the impact of milling on the shape and size was carried out through the structural analysis of Rietveld's refinements. The photoluminescence of the two Ln-doped samples were studied in terms of excitation, emission, CIE (x,y) chromaticities, lifetimes, and europium-quantum yields. The higher values of intrinsic quantum yield, strong red emission, and characteristic lifetimes at lower europium concentration were shown by **Eu@CWO**. Finally, the **Eu@CWO** was tested as chemical sensor towards toxic cations, based on the quenching effect of iron ions through an electron-transfer mechanism. The results verified the outstanding potential of **Eu@CWO** as highly stable optical material without previous activation and promising for the development of specific chemical sensors by a fast synthesis and "green" methodology.

Conflicts of interest

There are no conflicts to declare.

Acknowledgements

This work was supported by the Consejo Nacional de Investigaciones Científicas y Técnicas (CONICET) and Universidad Nacional de San Luis (Projects: PIP_CONICET 820CO and PROICO 02-2016). G.E.G. thanks the Fulbright Program for supporting his visit to Georgetown University. C.A.L. acknowledges ANPCyT (Project PICT 2014-3576). R.L.A. thanks the DOD-SMART fellowship, and K.E.K. recognizes the Clare Boothe Luce Foundation for support.

References

1 K. Binnemans, *Chem. Rev.*, 2009, **109**, 4283–4374.
2 C. D. S. Brites, P. P. Lima, N. J. O. Silva, A. Millán, V. S. Amaral, F. Palacio and L. D. Carlos, *New J. Chem.*, 2011, **35**, 1177.
3 L. D. Carlos, R. A. S. Ferreira, V. de Z. Bermudez and S. J. L. Ribeiro, *Adv. Mater.*, 2009, **21**, 509–534.
4 J.-C. G. Bünzli, S. Comby, A.-S. Chauvin and C. D. B. Vandevyver, *J. Rare Earths*, 2007, **25**, 257–274.
5 E. G. Moore, A. P. S. Samuel and K. N. Raymond, *Acc. Chem. Res.*, 2009, **42**, 542–552.
6 J.-C. G. Bünzli, *Chem. Rev.*, 2010, **110**, 2729–2755.
7 J. Liu, A. M. Kaczmarek, J. Billet, I. Van Driessche and R. Van Deun, *Dalt. Trans.*, 2016, **45**, 12094–12102.
8 J. Huang, Q. Li, J. Wang, L. Jin, B. Tian, C. Li, Y. Shi, Z. Wang and J. Hao, *Dalt. Trans.*, 2018, **47**, 8611–8618.
9 Y. Xie, S. Ma, Y. Wang, M. Xu, C. Lu, L. Xiao and S. Deng, *Opt. Mater. (Amst).*, 2018, **77**, 13–18.
10 R. Saraf, C. Shivakumara, N. Dhananjaya, S. Behera and H. Nagabhushana, *J. Mater. Sci.*, 2015, **50**, 287–298.
11 A. Xie, X. Yuan, S. Hai, J. Wang, F. Wang and L. Li, *J. Phys. D. Appl. Phys.*, 2009, **42**, 105107.
12 A. Khanna and P. S. Dutta, *J. Solid State Chem.*, 2013, **198**, 93–100.
13 Z. H. Zhang, Q. Huang, X. Zhao and Z. L. Huang, *Phys. status solidi*, 2009, NA-NA.
14 J. Zhang, L. Li, W. Zi, N. Guo, L. Zou, S. Gan and G. Ji, *J. Phys. Chem. Solids*, 2014, **75**, 878–887.
15 C. Du, F. Lang, Y. Su and Z. Liu, *J. Colloid Interface Sci.*, 2013, **394**, 94–99.
16 Z. Zhou, Y. Yu, X. Liu, W. Ye, G. Hu, B. Lei and Y. Yan, *J. Adv. Ceram.*, 2015, **4**, 318–325.
17 J. Liu, A. M. Kaczmarek and R. Van Deun, *J. Lumin.*, 2017, **188**, 604–611.
18 L. Yun, W. Shi-yu, L. Jin-yang and S. Xiao-lei, *Chinese J. Lumin.*, 2014, **35**, 1201–1204.
19 Y. Ouyang, X. Zhang, J. Wang, X. Wang and X. He, *Cailiao Daobao/Materials Rev.*, 2016, **30**, 33–37 and 56.
20 H. M. NOH, E. O. KIM, J. H. JEONG, K. R. KANG, Y. J. KIM, K. C. LEE, J. H. LEE, Y. D. PARK and J. H. KIM*, *New Phys. Sae Mulli*, 2014, **64**, 717–722.
21 C. Li, C. Lin, X. Liu and J. Lin, *J. Nanosci. Nanotechnol.*, 2008, **8**, 1183–1190.
22 S. Yan, J. Zhang, X. Zhang, S. Lu, X. Ren, Z. Nie and X. Wang, *J. Phys. Chem. C*, 2007, **111**, 13256–13260.
23 T. Rojac, M. Kosec, B. Malič and J. Holc, *J. Eur. Ceram. Soc.*, 2006, **26**, 3711–3716.
24 H. M. Rietveld, *J. Appl. Crystallogr.*, 1969, **2**, 65–71.
25 J. Rodríguez-Carvajal, *Phys. B Condens. Matter*, 1993, **192**, 55–69.
26 P. Thompson, D. E. Cox and J. B. Hastings, *J. Appl. Crystallogr.*, 1987, **20**, 79–83.
27 R. M. Hazen, L. W. Finger and J. W. E. Mariathasan, *J. Phys. Chem. Solids*, 1985, **46**, 253–263.
28 M. Keskar, S. K. Gupta, R. Phatak, S. Kannan and V. Natarajan, *J. Photochem. Photobiol. A Chem.*, 2015, **311**, 59–67.
29 P. Hänninen and H. Härmä, *Lanthanide Luminescence*, Springer Berlin Heidelberg, Berlin, Heidelberg, 2011, vol. 7.
30 A. Beeby, I. M. Clarkson, R. S. Dickins, S. Faulkner, D. Parker, L. Royle, A. S. de Sousa, J. A. G. Williams and M. Woods, *J. Chem. Soc. Perkin Trans. 2*, 1999, 493–504.
31 A. Chauvin, F. Gumy, D. Imbert and J. G. Bünzli, *Spectrosc. Lett.*, 2004, **37**, 517–532.
32 J.-C. G. Bünzli and C. Piguet, *Chem. Soc. Rev.*, 2005, **34**,

View Article Online
DOI: 10.1039/C9DT02109D

1048.
33 B. Chen, L. Wang, F. Zapata, G. Qian and E. B. Lobkovsky, *J. Am. Chem. Soc.*, 2008, **130**, 6718–6719.
34 Y. Yu, J.-P. Ma and Y.-B. Dong, *CrystEngComm*, 2012, **14**, 7157.
35 H. Xu, X. Rao, J. Gao, J. Yu, Z. Wang, Z. Dou, Y. Cui, Y. Yang, B. Chen and G. Qian, *Chem. Commun.*, 2012, **48**, 7377.
36 S. Pramanik, C. Zheng, X. Zhang, T. J. Emge and J. Li, *J. Am. Chem. Soc.*, 2011, **133**, 4153–4155.
37 Y.-T. Liang, G.-P. Yang, B. Liu, Y.-T. Yan, Z.-P. Xi and Y.-Y. Wang, *Dalt. Trans.*, 2015, **44**, 13325–13330.
38 X. Cheng, L. Jing, Y. Zhao, S. Du, J. Ding and T. Zhou, *J. Mater. Chem. C*, 2018, **6**, 1579–1586.

For Table of Contents Only

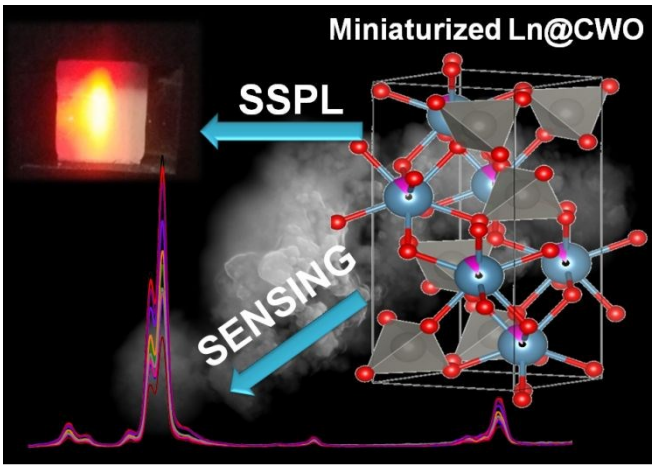

Two new nanosized lanthanide-doped materials (Sm and Eu) obtained by high-energy milling showed a suitable platform with solid-state photoluminescence properties for sensing applications.